Non-noble metal Cu as a cocatalyst on TiO_2 nanorod for highly efficient photocatalytic hydrogen production

Wei Chen[a*], Yanhong Wang[a], Shuang Liu[a], Li Gao[a], Liqun Mao[a], Zeyun Fan[b], Wenfeng Shangguan[b], Zheng Jiang[c]

a Henan Engineering Research Center of Resource & Energy Recovery from Waste, Henan University, Kaifeng 475004, PR China

b Research Center for Combustion and Environmental Technology, Shanghai Jiao Tong University, Shanghai 200240, PR China

c Faculty of Engineering and the Environment, University of Southampton, Highfield, Southampton SO17 1BJ, UK

Abstract: Nanorod-like TiO_2 photocatalysts with controllable particle size for hydrogen production were synthesized based on $H_2Ti_3O_7$ precursors using hydrothermal and ion exchange methods. The characteristics of TiO_2 photocatalysts, such as morphology, specific areas and crystalline quality, can be adjusted by changing hydrothermal conditions, thus optimizing its photocatalytic activity for hydrogen evolution. The TiO_2 nanorod possesses the highest photocatalytic activity, even higher than P25, when the hydrothermal temperature is 140 ^oC, which should be ascribed to its large specific area and good crystalline quality. Non-noble metal Cu as a substitute of Pt was loaded on the surface of TiO_2 nanorod to promote the photocatalytic hydrogen production. It was confirmed that, during the photocatalytic reaction process, Cu^0 rather than CuOx acted as active sites to enhance the photocatalytic activity. The highest photocatalytic H_2 evolution rate of Cu/TiO_2 reaches 1023.8 $\mu mol \cdot h^{-1}$ when the amount of loading is 0.1 wt%, reaching the 20 times of that of bare TiO_2(49.4 $\mu mol \cdot h^{-1}$) and approaching that of Pt/TiO_2(1161.7 $\mu mol \cdot h^{-1}$). Non-noble metal Cu not only facilitated the separation of carriers, but reduced the overpotential of hydrogen evolution, thus promoting the photocatalytic activity for hydrogen production.

Keywords: Photocatalyst; Hydrogen production; TiO_2 nanorod; Cu loading.

Introduction

Photocatalytic H_2 production has been considered to be a promising method to solve the problems of environmental pollution and the shortage of fossil fuels[1-3]. The preparation of the photocatalysts with high activity and low cost plays very important role in this filed. To date, a wide range of semiconductor photocatalysts such as TiO_2[4-6], $SrTiO_3$[7,8], CdS[9-12], GaN: ZnO[13], C_3N_4[14-17] have been investigated in relation to H_2 production. Among the reported photocatalysts, TiO_2 is recognized as a good candidate for photocatalytic H_2 production due to its characteristics of appropriate energy band position, non-toxicity, high chemical stability and low cost[18].

Recently, $H_2Ti_3O_7$ nanotubes have attract much attention because of their special structure and large specific surface, which have potential for application in environmental purification, gas sensors and photocatalysis, etc[19-21]. Interestingly, the particle size of $H_2Ti_3O_7$ nanotubes can be controlled by hydrothermal conditions. Also, with the same TiO_6 octahedron unit as TiO_2, $H_2Ti_3O_7$ is able to converts into TiO_2 nanorod with similar morphology and particle size under moderate treatment conditions[22]. Therefore, it is a feasible attempt to obtain TiO_2 nanorod with controllable particle size from $H_2Ti_3O_7$ nanotubes. It has been reported that, with respect to the TiO_2 nanoparticles, elongated and anisotropic TiO_2 nanorods can significantly reduce the probability of the interparticle hopping transport of electrons by providing better connectivity, thus possessing high photocatalytic activity[23]. Moreover, the particle size (specific surface area) and crystalline quality of photocatalytic materials play very important roles in photocatalytic activity for H_2 evolution[24]. Therefore, it is probably to obtain TiO_2 nanorods with high photocatalytic activity by adjusting its particle size (specific surface area) and crystalline quality based on $H_2Ti_3O_7$ nanotubes.

Generally speaking, if a photocatalytic reaction occurs, the photocatalyst not only needs appropriate energy band potential (including the demands of band gap and energy band position), but has abundant active sites on its surface for H_2 evolution. Although TiO_2 possesses appropriate energy band potential, its photocatalytic activity is low due to fast charge carrier recombination. To enhance the photocatalytic activity, noble metals such as Pt[25,26],Au[27]are loaded on the surface of TiO_2 as cocatalysts to facilitate the separation of photogenerated carrier. However, taking into account the high cost and rareness of noble metals, non noble metals are regarded as

more desirable cocatalysts for practical application. Most recently, Cu−containing species (e.g. Cu[28], CuO_x[29-31], CuO[32], $Cu(OH)_2$[33] and $Cu_2(OH)_2CO_3$[34]) as cocatalysts loaded on TiO_2 exhibit significant effect on enhancing the photocatalytic H_2 production. Huang et al [29]reported that, in the CuO_x/TiO_2 system, Cu_2O instead of CuO, plays the key role in promoting the photocatalytic activity. In the photocatalytic reaction process, CuO was reduced to Cu_2O by photogenerated electrons. The electrons in the conduction band of Cu_2O migrate to the conduction band of TiO_2 while the holes in valence band of TiO_2 to the valence band of Cu_2O, thus facilitating the separation of carriers. Yu et al[33]reported that the H_2 production of $Cu(OH)_2/TiO_2$ was remarkably enhanced compared to bare TiO_2 because the $Cu(OH)_2$ and Cu nanoparticles captured the electrons generated from TiO_2 and suppressed the recombination of electrons and holes. However, owing to that Cu species tend to be reduced or oxidized during the photocatalytic reaction process, the impact of single/pure Cu metal (Cu^0) without the change of chemical valence on promoting photocatalytic activity for hydrogen evolution is less well understood and still need to be investigated.

Herein, we prepared TiO_2 nanorod photocatalysts based on $H_2Ti_3O_7$ nanotube precursors to obtain TiO_2 with high photocatalytic activity. The particle size and crystalline quality of TiO_2 nanorods were adjusted by changing the hydrothermal temperatures used for preparing $H_2Ti_3O_7$. The dependence of the morphology of TiO_2 and photocatalytic activity for H_2 production was checked. Meanwhile, Cu metal (Cu^0) as a cocatalyst was loaded on TiO_2 nanorod *via* in situ photodeposition to promote the photocatalytic activity of TiO_2. The Cu^0 nanoparticles as active sites for H_2 evolution to remarkably enhance photocatalytic activity were verified. The optimum loading amounts of Cu on TiO_2 nanorods were studied. The roles of Cu in promoting the photocatalytic activity for hydrogen evolution were investigated as well.

Experimental section

Material synthesis

P25 composed of anatase 80% and rutile 20% was procured from Degussa Corporation, Germany, and others were procured from Sinopharm Chemical Reagent Co. Ltd. All materials were obtained from commercial sources and used without further purification.

$H_2Ti_3O_7$ was prepared by hydrothermal and ion-exchange methods[22, 27, 35]. Typically, 0.4 g P25 was added into 35 ml 10 $mol \cdot L^{-1}$ NaOH aqueous solutions. After stirring for 1 h at room

temperature, the mixture was transferred into a 50 ml sealed Teflon autoclave and heated at 110−180 ^{o}C for 60 h. The white precipitate at the bottom of Teflon autoclave was collected by centrifugation and washed repeatedly with deionized water to remove unreacted NaOH. After drying at 60 ^{o}C for 10 h, $Na_2Ti_3O_7$ was obtained. Subsequently, 1.0 g $Na_2Ti_3O_7$ was added in 200 ml 0.1 mol·L^{-1} HCl aqueous solutions for 48 h and then was washed repeatedly with deionized water until the neutral pH value. The finally obtained $H_2Ti_3O_7$ was dried at 60 ^{o}C for 10 h. The TiO_2 nanorod photocatalysts were obtained by calcination of $H_2Ti_3O_7$ nanotubes at 500 ^{o}C for 2 h with a ramping rate of 5 ^{o}C·min^{-1}.

Loading Cu on TiO_2 was achieved by an in situ photodeposition method. 0.1 g TiO_2 with 65 ml methanol solution(10 vol.%) containing a certain amount of $Cu(CH_3COO)_2$ was put into a 300 ml quartz reaction cell. The reaction cell was deaerated by a vacuum pump before reactions. Under the irradiation by a 300 W Xe lamp, the electrons of TiO_2 photogenerated by UV light (λ>200 nm) reduced and loaded Cu on the surface of TiO_2. After reaction 2 h, Cu/TiO_2 was collected by filtration and dried at 40 ^{o}C for 10 h.

Characterization

The crystal structure of the photocatalytic materials was confirmed by X-ray diffraction (Bruker-AXS Germany, Cu *Kα*, λ=0.15406 nm, 40 kV, 40 mA). The UV–vis diffuse reflection spectra (DRS) were determined by a UV–vis spectrophotometer Lambda 950 (PerkinelmerPE, USA) and were converted to absorbance by the Kubelka–Munk method. The morphology of the samples was studied by scanning electron microscopy (JSM 7610F, Japan). The transmission electron microscopy (TEM) measurements were conducted using a JEM-2100F (Japan) The specific areas of photocatalytic materials were determined by a BET method from N_2 absorption isotherms at 77 K (Micromeritics TriStarII3020 USA). The surface electronic state was analyzed by X-ray photoelectron spectroscopy (XPS, Shimadzu-Kratos, Axis UltraDLD, Japan). All the binding energy (BE) values were calibrated by using the standard BE value of contaminant carbon (C1s = 284.8 eV) as a reference.

Eelectrochemical measurements

The electrochemical measurements for linear sweep voltammetry (LSV) were performed using a CHI660D electrochemical work-station with three-electrode system according to our previous report[36]. In this study, all potentials were converted into the potentials of reversible hydrogen

electrode (RHE) by $E_{RHE} = E_{Ag/AgCl} + 0.197 + 0.059 \times pH$. The photocatalysts electrodes as the working electrodes were prepared by coating paste onto FTO glasses with an area of about 1 cm×1.5 cm. The working electrodes were prepared as follow: 5 mg ground powder was immersed into 1 ml of 0.1 wt% nafion solution to obtain viscous slurry. 250 µl slurry was then injected onto FTO glass and was dried in air at 80 ^{o}C for 2 h. Measurements were performed using a quartz electrochemical cell with a Pt wire as a counter electrode and an Ag/AgCl as a reference electrode. The effective surface area of the electrodes was about 1 cm×1 cm.

Photocatalytic reactions

Photocatalytic reactions for hydrogen evolution were carried out in a 350 ml top irradiation reaction Pyrex flask at ambient temperature. The catalyst powder (50 mg) was suspended in 65 ml methanol solution(20 vol%) under magnetic stirring. The reaction cell was connected to a vacuum system, and a 300 W Xe lamp (λ> 300 nm) was used as a light source. The gases evolved were analyzed by GC with a TCD detector (Huaai, GC9560, China, MS-5A, argon as carrier gas).

Results and discussion

Crystalline structures, morphologies, BET and DRS of TiO_2

The XRD patterns of TiO_2 samples prepared under different hydrothermal temperatures are shown in Fig. 1. As shown in Fig. 1, after heat treatment at 500 ^{o}C, TiO_2 samples prepared under 110 – 160 ^{o}C hydrothermal temperatures exhibit only the anatase phase, while the sample under 180 ^{o}C hydrothermal temperature exhibits monoclinic phase (JCPDS 46 – 1237), named TiO_2(B). Of note, the diffraction peaks of TiO_2 become sharp as hydrothermal temperatures rise, suggesting that the crystallization of TiO_2 proceeds gradually with increasing the hydrothermal temperatures used for precursor $H_2Ti_3O_7$.

Fig. 2 shows the SEM and TEM images of TiO_2 samples prepared at different hydrothermal temperatures. After calcination 500 ^{o}C, the TiO_2 samples prepared at 180 ^{o}C hydrothermal temperature show nanorod morphology with lengths of longer 3 µm and diameters of about 200 nm. With decreasing hydrothermal temperature from 180-110 ^{o}C, the size of TiO_2 nanorod becomes smaller. The lengths of TiO_2 nanorods prepared 110-140 ^{o}C are only 30-50 nm and the diameters are 5-10 nm. During the hydrothermal process, the Ti-O-Ti bonds of TiO_2 are broken and form unstable $[Ti(OH)_6]^{2-}$, subsequently combine to nuclei by oxolation and olation. The nuclei grow to thin plates and scroll up into $Na_2Ti_3O_7$ nanotubes[19]. Under high hydrothermal

temperature, the growth rate of nuclei for nanosheets is fast and leads to the large size of $Na_2Ti_3O_7$ nanotubes, which finally results in the large size of TiO_2. In addition, Marchand reported that[37], during heat treatment process, the hydrogen titanate transformed into TiO_2(B) firstly and then into TiO_2 anatase with the increase of the calcination temperatures. Therefore, the TiO_2 sample hydrothermal temperatures at 180 ^oC exhibits TiO_2(B) rather than anatse because its particle size is too large to fail to transform TiO_2(B) into anatase under 500 ^oC calcination. The specific surface areas of photocatalytic materials, as listed in table 1, increase with the decreasing of hydrothermal temperatures. This result is consistent with the SEM analysis, in which the length of nanobelt or nanorod decreases from 300 to 40 nm corresponding to the specific surface areas increasing from 24 to100 $m^2 \cdot g^{-1}$.

The DRS of TiO_2 samples prepared at different hydrothermal temperatures are shown in Fig. 3. The absorption edge of TiO_2 hydrothermal temperatures at 180 ^oC is 410 nm, corresponding to band gap of 3.0 eV, which is good agreement with that of TiO_2(B) reported by Tributsch group[38]. The absorption edges of samples hydrothermal temperatures at 110 – 140 ^oC are about 380 nm, which are typically absorption edges of anatase. These results are also consistent with the XRD analysis.

Influence of hydrothermal temperature on photocatalytic activity of TiO_2 nanorod

The table 1 shows the hydrogen evolution rates of TiO_2 photocatalysts with 0.3 wt% Cu loading. The reaction was performed in the methanol solution containing 0.05 g catalyst under UV irradiation (λ> 300 nm). It is clear that, with the decrease of the hydrothermal temperatures(140 −180 ^oC), the rates of photocatalytic hydrogen evolution on TiO_2 samples increase along with the increase of the specific surface areas. The highest hydrogen evolution rate is up to 975.6 $\mu mol \cdot h^{-1}$ when the hydrothermal temperature is 140 ^oC, which is even more than that of the P25. However, a further decrease of hydrothermal temperatures would lead to decrease in photocatalytic hydrogen production. The hydrogen evolution rate of TiO_2 prepared by 110 ^oC is only 602.1 $\mu mol \cdot h^{-1}$ even though its specific surface area reaches up to 104.6 $m^2 \cdot g^{-1}$.

As we know, both the high specific surface area and the high crystalline quality of photocatalysts are beneficial for their photocatalytic performance. Under the high hydrothermal temperatures, the specific surface areas are too low to provide the enough active sites for hydrogen evolution. In contrast, under the low hydrothermal temperatures, the crystalline quality is low and

results in the recombination of charge carriers on the crystal defects. Therefore, the high activity for hydrogen evolution of the sample prepared by hydrothermal temperature at 140 ^{o}C should be ascribed to the high specific surface area and relatively high crystalline quality. To further exhibit the dependence of the crystalline quality on photocatalytic activity regardless of the specific surface area, the data of the surface-specific hydrogen yields are also listed in table 1. When hydrothermal temperatures are lower than 160 ^{o}C, surface-specific hydrogen yields increase with the increase of the hydrothermal temperatures, suggesting that good crystalline quality is benefit to photocatalytic activity. Surprisingly, surface-specific hydrogen yields of TiO_2 prepared by 180^{o}C and 160 ^{o}C are lower than that of TiO_2 prepared at 140 ^{o}C and 120 ^{o}C although the crystalline quality of the former is better than that of the latter. Generally, to avoid the intense recombination in the migration process of electrons and holes, the migration path of carriers from bulk to surface should be short(<100 nm)[39, 40]. In other words, photocatalytic activity of photocatalysts will be strongly limited if its particle size is too large (>200 nm). In this situation, the advantage of TiO_2 photocatalyst prepared by 180 ^{o}C and 160 ^{o}C in good performance of separation carriers is weakened due to large particle size and leads to the lower surface-specific hydrogen yields. In addition, it is found that the surface-specific hydrogen yield of P25 is much higher than that of TiO_2 nanorod, which is attributed to its anatase – rutile – phase junctions[41].

Influence of Cu loading on photocatalytic activity of TiO_2 nanorod

Fig. 4 shows the XRD patterns of TiO_2 nanorod prepared by 140 ^{o}C hydrothermal temperature with different amounts of Cu loading. After loading, there is no change in TiO_2 diffraction peaks, indicating Cu loads on the surface of TiO_2 rather than incorporates into the lattice of TiO_2. Additionally, no characteristic diffraction peaks of Cu was observed when the loading amounts were 0.1 wt% – 1 wt%, which be ascribed to low loading amounts and/or small size of Cu particles. Of note, the diffraction peaks at 40.3^{o} and 50.5^{o}, which are attributed to (111) and (200) plane of the cubic phase Cu metal (Cu^0) (JCPDS 65–9026), could be observed as the loading amount reached 3 wt %, implying the photogenerated electrons of TiO_2 nanorod had ability to reduce the Cu^{2+} to Cu^0.

To investigate the morphologies of Cu/TiO_2 and the distribution state of Cu on the surface of TiO_2, TEM is employed and images of 1 wt%Cu/TiO_2 are shown in Fig.5. Cu/TiO_2 remains on nanorod structure as shown in Fig. 5A. The SAED patterns exhibit the anatase structure of

TiO_2(Fig.5B). From both the TEM image and SAED patterns, the presence of Cu was not observed, but the EDS mapping(Fig. 5C-F) confirmed Cu was loaded on the surface of TiO_2 successfully. In addition, element content analysis of EDS (Fig. 5G) shows that the ratio of Cu and Ti/O contents has not notable change at linear scanning range from 0 to 800 nm, indicating that Cu particles disperse on the surface of TiO_2 homogeneously. The absence of Cu from the TEM image and SAED patterns should be due to the low loading amount as well as low discrimination of Cu and TiO_2.

To further investigate the chemical states loaded on the surface of TiO_2, especially under low loading amounts, the Cu binding energies of Cu/TiO_2 with 0.1 wt% and 1wt% loading amounts were measured by XPS(Fig. 6). As shown in Fig. 6, both Cu/TiO_2 photocatalysts exhibit Cu $2p_{3/2}$ and Cu $2p_{1/2}$ peaks at 931.8 eV and 951.9 eV, respectively, which can be assigned to Cu^0/Cu^+[42]. No characteristic satellite peak of Cu^{2+} at about 942.5 eV is observed, suggesting that Cu on the surface of TiO_2 with low loading amounts also presents reduced sate. Based on the XPS and XRD results, it could be determined that, in the photodeposition process, the Cu ions were reduced to Cu^0 by photogenerated electrons and acted as active sites for hydrogen evolution.

The DRS of TiO_2 nanorod with different Cu loading amounts are shown in Fig. 7. Compared to the pure TiO_2, the absorption band edges of Cu/TiO_2 at 380 nm have no obvious change, which is also because the Cu is loaded on the surface of TiO_2 rather than doped in its crystal lattice. However, with the increase of Cu loading contents, the new absorption of Cu/TiO_2 longer 380 nm can be observed, which should be assigned to absorption of Cu. The result also indicates the Cu is loaded on the photocatalysts successfully.

Fig. 8 shows the hydrogen evolution rates of TiO_2 nanorod prepared by hydrothermal temperature at 140 ^oC with different amounts of Cu loading. Bare TiO_2 exhibits low photocatalytic activity for hydrogen production due to strong recombination of electrons and hole. After Cu loading, the hydrogen evolution rate is significantly promoted because Cu particles provide the active sites for hydrogen evolution. When the loading amount is 0.1 wt%, the highest photocatalytic evolution rate reaches 1023.8 $\mu mol \cdot h^{-1}$, even 20 times that of bare TiO_2, which approaches that of Pt/TiO_2(1161.7 $\mu mol \cdot h^{-1}$). Based on this work and the previous reports of Cu species loaded TiO_2 for photocatalytic hydrogen production (shown in table 2), it is clear that Cu is an effective cocatalyst to promote photocatalytic hydrogen production activity. Also, as

non-noble-metal, Cu is a good candidate to substitute Pt or Au for reducing the cost of photocatalysts. However, a further increase of Cu loading amount will lead to a decrease of photocatalytic hydrogen evolution rate.

To clarify the effect of Cu on improving the photocatalytic activity for hydrogen evolution, the hydrogen evolution reaction (HER) of bare TiO_2 and Cu/TiO_2 was carried out by a linear sweep voltammetry (LSV) method(Fig. 9). From the LSV curves, it can be observed that, compared to the bare TiO_2, the current densities of Cu/TiO_2 are apparently enhanced, indicating Cu/TiO_2 possess higher activity of HER. Additionally, it is noteworthy that the polarization curves of Cu/TiO_2 with different Cu loading amounts (0.1 wt% – 1 wt%) show lower onset potentials of hydrogen evolution than that of bare TiO_2, suggesting the overpotential of hydrogen evolution on Cu/TiO_2 is less than that on bare TiO_2 [47]. Generally, metal cocatalysts with high work function (e.g. Pt, Au, Cu) are able to enhance the separation of electrons and holes by means of forming schottky barrier junction with photocatalyst. Therefore, Cu loading on TiO_2 not only facilitates the separation of carriers, but reduces the overpotential of hydrogen evolution, thus promoting the photocatalytic activity for hydrogen production. Moreover, the overpotential of hydrogen evolution on TiO_2 with 0.1 wt% Cu loading is only 0.40 V, lower than that of TiO_2 with 0.5 wt% and 1 wt% Cu loading (0.48 V), which may be because excessive Cu loading results in relative large particle size.

To examine the stability of Cu/TiO_2 photocatalysts, a time course of gas evolution on 0.3 wt% Cu/TiO_2 is shown in Fig.10. It can be seen that, as the reaction proceeds, the photocatalytic hydrogen rate declines slightly, especially after 12 h reaction. However, the declining trend was suppressed when 3 ml methanol was supplemented, implying that the decline of photocatalytic activity is due to the consumption of sacrifice reagent rather than the devitalization of the photocatalyst. Under the 36 h irradiation, the total amount of H_2 is 35.9 mmol and the turnover numbers (TON) reaches 28.5, indicating hydrogen is indeed generated in a photocatalytic reaction instead of chemical reaction process.

Conclusion

In summary, nanorod−likeTiO_2 photocatalysts with high photocatalytic activity was synthesized based on $H_2Ti_3O_7$ precursors using hydrothermal and ion exchange methods. The physical properties of TiO_2 photocatalysts can be controlled by adjusting the hydrothermal temperature.

The TiO_2 nanorod photocatalyst prepared at 140 ^oC possesses the highest photocatalytic activity for hydrogen production, which is even better than P25. Its good photocatalytic performance is attributed to the large specific area and relatively good crystalline quality. Non-noble metal Cu (Cu^0) loading on TiO_2 not only facilitates the separation of carriers, but reduces the overpotential of hydrogen evolution, thus significantly enhancing the photocatalytic activity. The highest photocatalytic H_2 evolution rate of Cu/TiO_2 reaches 1023.8 $\mu mol \cdot h^{-1}$ when the amount of loading is 0.1 wt%, which approaches that of Pt/ TiO_2. This work not only displays an idea to obtain photocatalysts with high photocatalytic activity for hydrogen production, but provides a possibility of reducing the cost of photocatalysts for the particle application of hydrogen production in the future.

Acknowledgements

This work was supported by the National Natural Science Foundation of China (51602091), the International Cooperation Project of Department of Science and Technology of Henan Province (162102410011) and Natural Science Foundation of Henan Province (182300410205).

References

[1] X. Li, J.G. Yu, J.X. Low, Y.P. Fang, J. Xiao, X.B. Chen, Engineering heterogeneous semiconductors for solar water splitting, J. Mater. Chem. A 3(2015) 2485 – 2534.

[2] P. Zhang, J. Zhang, J.L. Gong, Tantalum-based semiconductors for solar water splitting, Chem. Soc. Rev. 43(2014) 4395 – 4422.

[3] K. Maeda, Photocatalytic water splitting using semiconductor particles: History and recent developments, J. Photochem. Photobiol. C: Photochem. Rev. 12(2011) 237 – 268.

[4] A. Fujishima, K. Honda, Electrochemical photolysis of water at a semiconductor electrode, Nature 238(1972) 37 – 38.

[5] C.X. Zhao, H. Luo, F. Chen, P. Zhang, L.H. Yi, K. You, A novel composite of TiO_2 nanotubes with remarkably high efficiency for hydrogen production in solar-driven water splitting, Energy Environ. Sci. 7(2014) 1700 – 1707.

[6] B. C. Qiu, M.Y. Xing, J.L. Zhang, Mesoporous TiO_2 nanocrystals grown in situ on graphene aerogels for high photocatalysis and lithium-ion batteries, J. Am. Chem. Soc. 136(2014) 5852 – 5855.

[7] S.X. Ouyang, H. Tong, N. Umezawa, J.Y. Cao, P. Li, Y.P. Bi, Y.J. Zhang, J.H. Ye, Surface-alkalinization-induced enhancement of photocatalytic H_2 evolution over $SrTiO_3$-based photocatalysts, J. Am. Chem. Soc. 134(2012) 1974 –1977.

[8] W. Chen, H. Liu, X.Y. Li, L.Q. Mao, Z.Y. Fan, W.F. Shangguan, W.J. Fang, Y.S. Liu, Polymerizable complex synthesis of $SrTiO_3$:(Cr/Ta) photocatalysts to improve photocatalytic water splitting activity under visible light, Appl. Catal. Environ. B 192(2016) 145 – 151.

[9] Q. Li, B.D. Guo, J.G. Yu, J.R. Ran, B.H. Zhang, H.J. Yan, J.R. Gong, Highly efficient visible-light-driven photocatalytic hydrogen production of CdS-cluster-decorated graphene nanosheets, J. Am. Chem. Soc. 133(2011) 10878 – 10884.

[10] H. Yan, J. Yang, G. Ma, G. Wu, X. Zong, Z.B. Lei, J.Y. Shi, C. Li, Visible-light-driven hydrogen production with extremely high quantum efficiency on Pt-PdS/CdS photocatalyst, J. Catal. 266(2009) 165 – 168.

[11] Q.Z. Wang, J.J. Li, Y. Bai, J. Lian, H. Huang, W.F. Shangguan, Photochemical preparation of Cd/CdS photocatalysts and its efficient photocatalytic hydrogen production under visible light irradiation, Green Chem. 16(2014) 2728 – 2735.

[12] B.C. Qiu, Q.H. Zhu, M.M. Du, L.G. Fan, M.Y. Xing, J.L. Zhang, Efficient solar light harvesting CdS/Co_9S_8 hollow cubes for Z-Scheme photocatalytic water splitting, Angew. Chem. Int. Ed. 56(2017) 2684 – 2688.

[13] K. Maeda, K. Teramura, D. Lu, T. Takata, N. Saito, Y. Inoue, K. Domen, Photocatalyst releasing hydrogen from water, Nature 440(2006) 295.

[14] X. Wang, K. Maeda, A. Thomas, K. Takanbe, G. Xin, J. Carlsson, K. Domen, M. Antonietti, A metal-free polymeric photocatalyst for hydrogen production from water under visible light, Nature Mater. 8(2009) 76 – 80

[15] S.P. Wang, C.J. Li, T. Wang, P. Zhang, A. Li, J.L. Gong, Controllable synthesis of nanotube-type graphitic C_3N_4 and their visible-light photocatalytic and fluorescent properties, J. Mater. Chem. A 2(2014) 2885 – 2890.

[16] F. He, G. Chen, Y.S. Zhou, Y.G. Yu, Y. Zheng, S. Hao, The facile synthesis of mesoporous g-C_3N_4 with highly enhanced photocatalytic H_2 evolution performance, Chem. Commun. 51(2015) 16244 – 16246.

[17] J. Yu, S. Wang, B. Cheng, Z. Lin, F. Huang, Noble metal-free $Ni(OH)_2$–gC_3N_4 composite

photocatalyst with enhanced visible-light photocatalytic H_2-production activity, Catal. Sci. Technol. 3(2013) 1782 – 1789.

[18] Y. Ma, X.L. Wang, Y.S. Jia, X.B. Chen, H.X. Han, C. Li, Titanium dioxide-based nanomaterials for photocatalytic fuel generations, Chem. Rev. 114(2014) 9983 – 10043.

[19] Y. Wang, G. Du, H. Liu, D. Liu, S. Qin, N. Wang, C. Hu, X. Tao, J. Jiao, J. Wang, Nanostructured sheets of Ti-O nanobelts for gas sensing and antibacterial applications, Adv. Funct. Mater, 18(2008) 1131–1137.

[20] Q. Chen, W.Z. Zhou, G.H. Du, L.M. Peng, Trititanate nanotubes made via a single alkali treatment, Adv. Mater. 14(2002)1208 – 1211.

[21] C. L. Li, J. Yuan, B.Y. Han, L. Jiang, W.F. Shangguan, TiO_2 nanotubes incorporated with CdS for photocatalytic hydrogen production from splitting water under visible light irradiation, Int. J. Hydrogen Energy 35(2010) 7073 – 7079.

[22] Y. Liu, Z.L. Wang, W.D. Wang, W.X. Huang, Engineering highly active TiO_2 photocatalysts via the surface-phase junction strategy employing a titanate nanotube precursor. J. Catal. 310 (2014) 16 – 23.

[23] S.S. Li, C.P. Chang, C.C. Lin, Y.Y. Lin, C.H. Chang, J.R. Yang, M. W. Chu, C.W. Chen, Interplay of three-dimensional morphologies and photocarrier dynamics of polymer/TiO_2 bulk heterojunction solar cells, J. Am. Chem. Soc. 133(2011)11614 – 11620.

[24] A. Kudo, Y. Miseki. Heterogeneous photocatalyst materials for water splitting, Chem. Soc. Rev. 38(2009) 253 – 278.

[25] J.H. Yang, D.G. Wang, H.X. Han, C. Li, Roles of cocatalysts in photocatalysis and photoelectrocatalysis, Acc. Chem. Res. 46(2013) 1900 – 1909.

[26] J. Pan, G. Liu, G.Q. Lu, H.M. Cheng, On the true photoreactivity order of {001}, {010}, and {101} facets of anatase TiO_2 crystals, Angew. Chem. Int. Ed. 50(2011) 2133 – 2137.

[27] A. Dosado, W.T. Chen, A. Chan, D. Waterhouse, G. Waterhouse, Novel Au/TiO_2 photocatalysts for hydrogen production in alcohol–water mixtures based on hydrogen titanate nanotube precursors, J. Catal. 330(2015) 238 – 254.

[28] D. Ni, H.Y. Shen, H.Q. Li, Y. Ma, T.Y. Zhai, Synthesis of high efficient Cu/TiO_2 photocatalysts by grinding and their size-dependent photocatalytic hydrogen production. Appl. Surf. Sci. 409(2017) 241 – 249.

[29] Z.L. Wang, Y. Liu, D. Martin, W.D. Wang, J.W. Tang, W.X. Huang, CuO_x–TiO_2 junction: what is the active component for photocatalytic H_2 production? Phys. Chem. Chem. Phys. 15(2013) 14956 – 14960.

[30] D. Kumar, N. Reddy, B. Srinivas, V. Durgakumari, V. Roddatis, O. Bondarchuk, M. Karthik, Y. Ikuma, M. Shankar, Stable and active Cu_xO/TiO_2 nanostructured catalyst for proficient hydrogen production under solar light irradiation, Sol Energy Mater Sol Cells 146(2016) 63 – 71.

[31] M. Jung, J. Scott, Y. Ng, Y. Jiang, R. Amal, CuO_x dispersion and reducibility on TiO_2 and its impact on photocatalytic hydrogen evolution, Int. J. Hydrogen Energy 39(2014) 12499 – 12506.

[32] D. Kumar, M. Shankar, M. Kumari, G. Sadanadam, B. Srinivas, V. Durgakumari, Nano-size effects on CuO/TiO_2 catalysts for highly efficient H_2 production under solar light irradiation, Chem. Commun. 49(2013) 9443 – 9445.

[33] J.G. Yu, J.R. Ran, Facile preparation and enhanced photocatalytic H_2-production activity of $Cu(OH)_2$ cluster modified TiO_2, Energy Environ. Sci. 4(2011)1364 – 1371.

[34] Z.K. He, J.W. Fu, B. Cheng, J.G. Yu, S.W. Cao, $Cu_2(OH)_2CO_3$ clusters: Novel noble-metal-free cocatalysts for efficient photocatalytic hydrogen production from water splitting, Appl. Catal. Environ. B 205(2017) 104 – 111.

[35] H.Y. He, J.H. Lin, W. Fu, X.L. Wang, Q.S. Zeng, Z. Liu, MoS_2/TiO_2 edge-on heterostructure for efficient photocatalytic hydrogen evolution, Adv. Energy Mater. 6(2016) 464 – 451.

[36] W. Chen, B.B. Yang, Q.T. Yu, L.Q. Mao, Z.Y. Fan, W.F. Shangguan, Effect of Rh oxide as a cocatalyst over $Bi_{0.5}Y_{0.5}VO_4$ on photocatalytic overall water splitting, Appl. Surf. Sci. 355(2015) 1069 – 1074.

[37] R. Marchand, L. Brohan, M. Tournoux, TiO_2(B) a new form of titanium dioxide and the potassium octatitanate $K_2Ti_8O_{17}$, Mat. Res. Bull. 15(1980) 1129 – 1133.

[38] G. Betz, H. Tributsch, Hydrogen insertion (intercalation) and light induced proton exchange at TiO_2(B)-electrodes, J. Appl. Electrochem. 14(1984) 315 – 322.

[39] S.L. Wang, S. Lin, D.Q. Zhang, G.S. Li, M. Leung, Controlling charge transfer in quantum-size titania for photocatalytic applications, Appl. Catal. Environ. B 215(2017) 85 – 92.

[40] J.Q. Bai, W. Wen, J.M. Wu, Facile synthesis of Ni-doped TiO_2 ultrathin nanobelt arrays with enhanced photocatalytic performance, CrystEngComm. 18(2016) 1847 – 1853.

[41] J. Zhang, Q. Xu, Z. Feng, M. Li, C. Li, Importance of the relationship between surface phases and photocatalytic activity of TiO_2, Angew. Chem. Int. Ed. 47(2008) 1766 – 1769.

[42] M. Wang, L. Sun, Z.Q. Lin, J.H. Cai, K.P. Xie, C.J. Lin, p–n Heterojunction photoelectrodes composed of Cu_2O-loaded TiO_2 nanotube arrays with enhanced photoelectrochemical and photoelectrocatalytic activities, Energy Environ. Sci. 6(2013) 1211 – 1220.

[43] W. Chen, H. Wang, L.Q. Mao, X.P. Chen, W.F. Shangguan, Influence of loading Pt, RhO_2 cocatalysts on photocatalytic overall water splitting over $H_{1.9}K_{0.3}La_{0.5}Bi_{0.1}Ta_2O_7$, Catal. Commun. 57(2014) 115 – 118.

[44] S. Obregón, M. Muñoz-Batista, M. Fernández-García, A. Kubacka, G. Colón, Cu-TiO_2 systems for the photocatalytic H_2 production: Influence of structural and surface support features, Appl Catal Environ B 2015; 179: 468 – 78.

[45] M. Dozzi, G. Chiarello, M. Pedroni, S. Livraghi, Elio Giamello, E. Selli, High photocatalytic hydrogen production on Cu(II) pre-grafted Pt/TiO_2, Appl Catal Environ B 2017; 209: 417 – 428.

[46] R. Rather, S. Singh, B. Pal, A Cu^{+1}/Cu^0-TiO_2 mesoporous nanocomposite exhibits improved H_2 production from H_2O under direct solar irradiation, J Catal 2017; 346: 1 – 9.

[47] A. Garcia-Esparza, D. Cha, Y.W. Ou, J. Kubota, K. Domen, K. Takanabe, Tungsten carbide nanoparticles as efficient cocatalysts for photocatalytic overall water splitting, Chemsuschem 6(2013) 168 – 181.

Figure and Table Captions

Table 1 Hydrogen evolution rates of TiO_2 photocatalysts prepared under different hydrothermal temperatures with 0.3 wt % Cu loading. Reaction conditions: 0.05 g catalyst, 300 W Xe lamp (λ>300 nm), 65 ml methanol solution (20 vol%).

Table 2 reported hydrogen evolution rates on TiO_2 photocatalysts loaded on Cu, Au or Cu/Pt.

Fig.1 XRD patterns of TiO_2 samples prepared under different hydrothermal temperatures and calcination of 500^oC.

Fig. 2 SEM and TEM images of TiO_2 samples prepared at different hydrothermal temperatures and calcination of 500^oC. SEM: 180^oC (A), 160 ^oC (B), 140 ^oC (C), 120^oC (D), 110^oC (E); TEM: 140 ^oC (F), 120^oC (G), 110^oC(H).

Fig. 3 DRS patterns of TiO_2 samples prepared under different hydrothermal temperatures and calcination of 500^oC.

Fig. 4 XRD patterns of TiO_2 nanorod prepared by 140 ^oC hydrothermal temperature with different amounts of Cu loading. A: 0.1 wt%, B: 0.3 wt%, C: 0.5 wt%, D: 1 wt%, E: 3 wt%.

Fig. 5 TEM images and EDS mappings of 1wt% Cu/TiO_2. A: TEM image of Cu/TiO_2, (B) SADE image of Cu/TiO_2, (C, D, E, F) EDS mappings of Cu/TiO_2 (G) relative elements content in the liner scanning area ("green line" in the C image).

Fig. 6 Cu binding energies of Cu/TiO_2 with 0.1 wt% and 1 wt% loading amounts.

Fig. 7 DRS of TiO_2 nanorod with different Cu loading amounts.

Fig. 8 Hydrogen evolution rates of TiO_2 nanorod prepared by hydrothermal temperature at 140 ^oC with different amounts of Cu loading. Reaction conditions: 0.05 g catalyst, 300 W Xe lamp (λ>300 nm), 65 ml methanol solution (20 vol%)

Fig. 9 Linear sweep voltammetry (LSV) curves of TiO_2 and Cu/TiO_2.

Fig. 10 Time course of hydrogen evolution on 0.3 wt% Cu/TiO_2. Reaction conditions: 0.1 g catalyst, 300 W Xe lamp (λ>300 nm), 65 ml methanol solution (20 vol%)

Table

hydrothermal temperatures/^{o}C	calcination temperature/^{o}C	crystalline phase	S_{BET}($m^2 \cdot g^{-1}$)	H_2 evolution rate	
				$\mu mol \cdot h^{-1}$	$\mu mol \cdot h^{-1} \cdot m^{-2}$
180	500	Monoclinic	24.5	150.3	122.7
160	500	Anatase	35.4	279	157.5
140	500	Anatase	101.2	975.6	192.6
120	500	Anatase	102.7	963.9	187.7
110	500	Anatase	104.6	602.1	115.2
P25	−	Anatase & Rutile	48.7	960.4	394.5

Table 2

No.	photocatalysts	Light source	Sacrificial reagent	H_2 evolution ($mmol \cdot h^{-1} \cdot g^{-1}$)	Ref.
1	$Cu(OH)_2$/P25	3 W UV-LED	Ethylene glycol	3.4	33
2	$Cu_2(OH)_2CO_3$/P25	300 W Xe lamp	Methanol	6.7	34
3	CuO_x/TiO_2(anatase)	125 W Hg lamp	Methanol	18.1	44
4	Pt/CuO/P25	300 W Xe lamp	Methanol	27.2	45
5	Cu/P25	300 W Xe lamp	Methanol	9.5	28
6	Cu /mp-TiO_2	Sunlight	Methanol	33.3	46
7	Au/TiO_2 nanorod	100 W Spectraline UV light	Methanol	14.4	27
8	Cu/TiO_2 nanorod	300 W Xe lamp	Methanol	20.4	This work

Figure 1

Click here to download Figure: Fig 1.docx

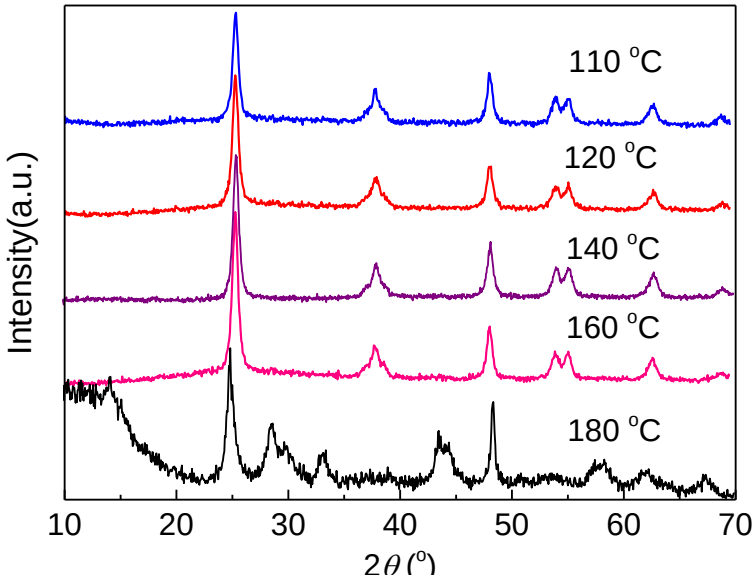

Figure 2

Click here to download Figure: Fig 2.docx

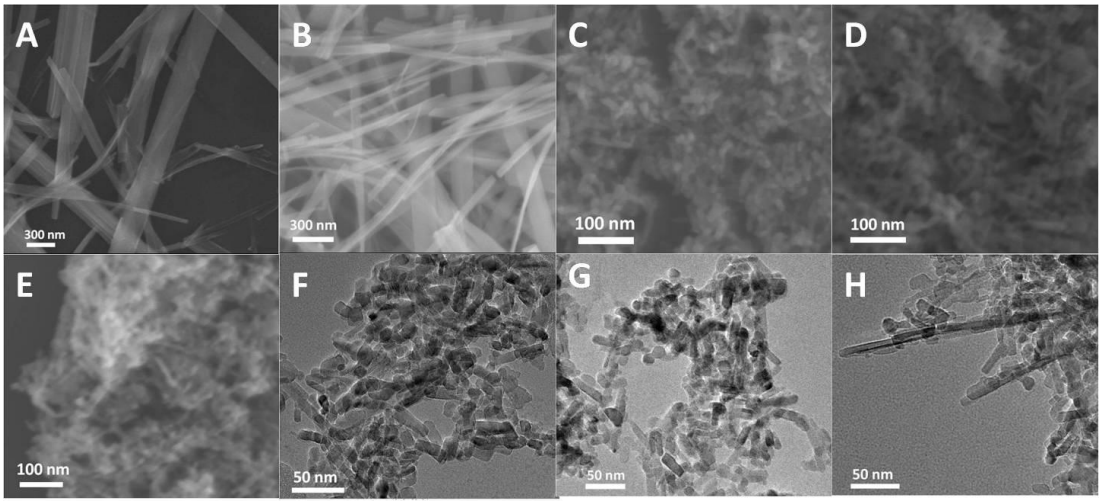

Figure 3

Click here to download Figure: Fig 3.docx

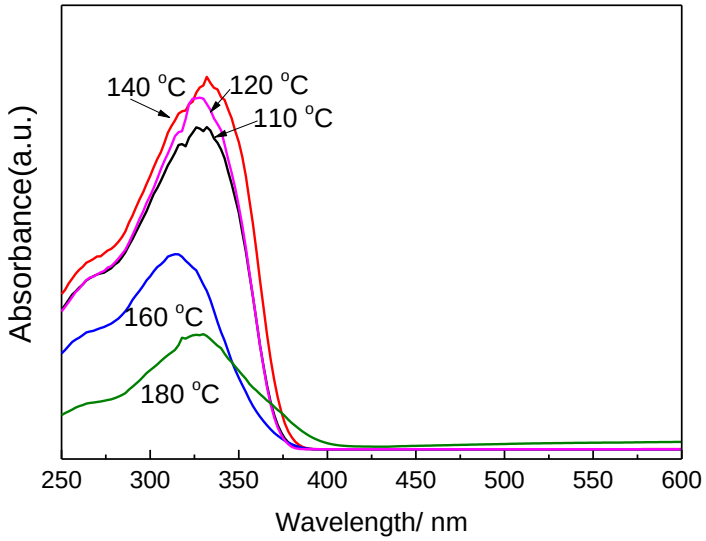

Figure 4

Click here to download Figure: Fig 4.docx

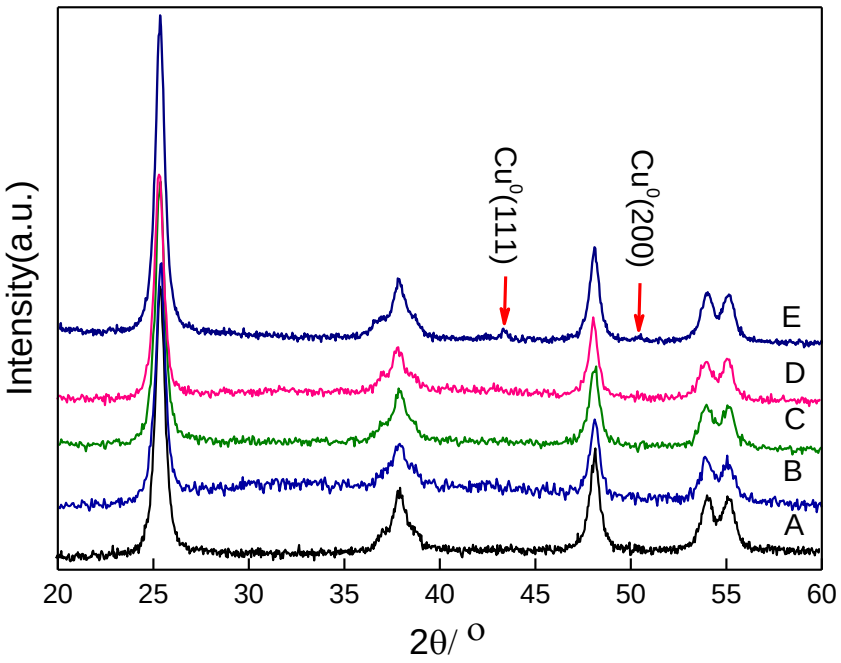

Figure 5

Click here to download Figure: Fig 5.docx

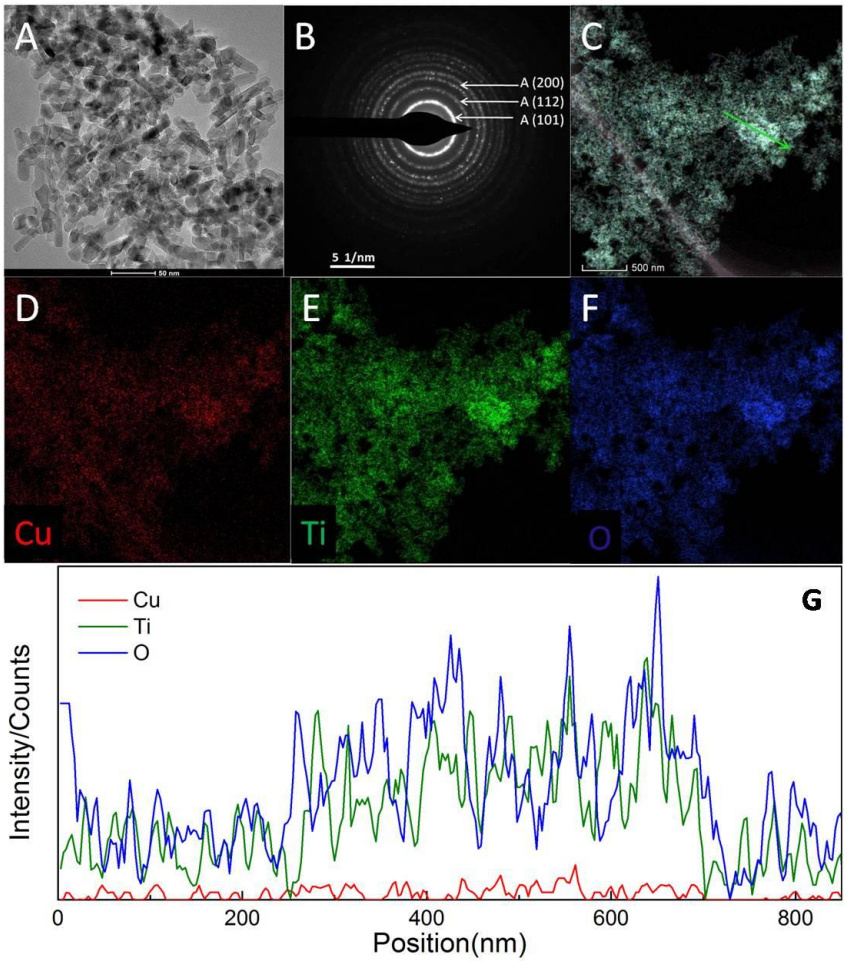

Figure 6

Click here to download Figure: Fig 6.docx

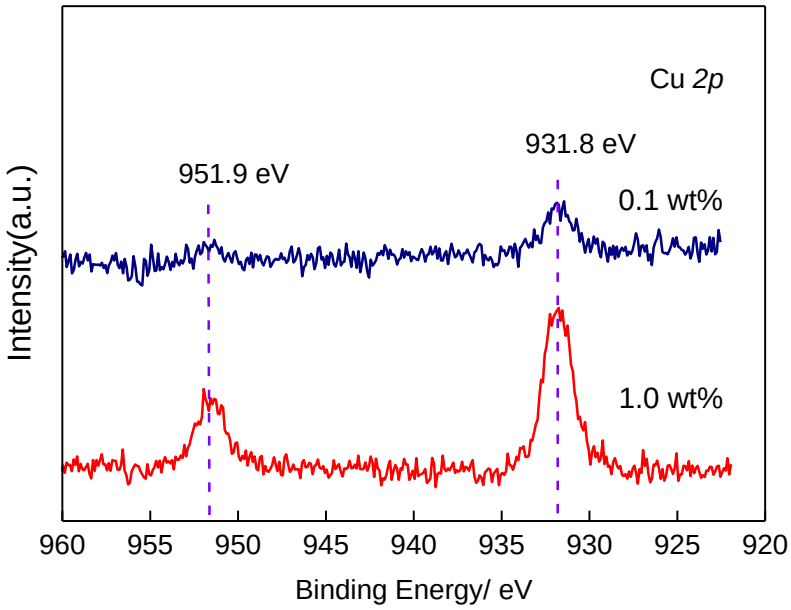

Figure 7

Click here to download Figure: Fig 7.docx

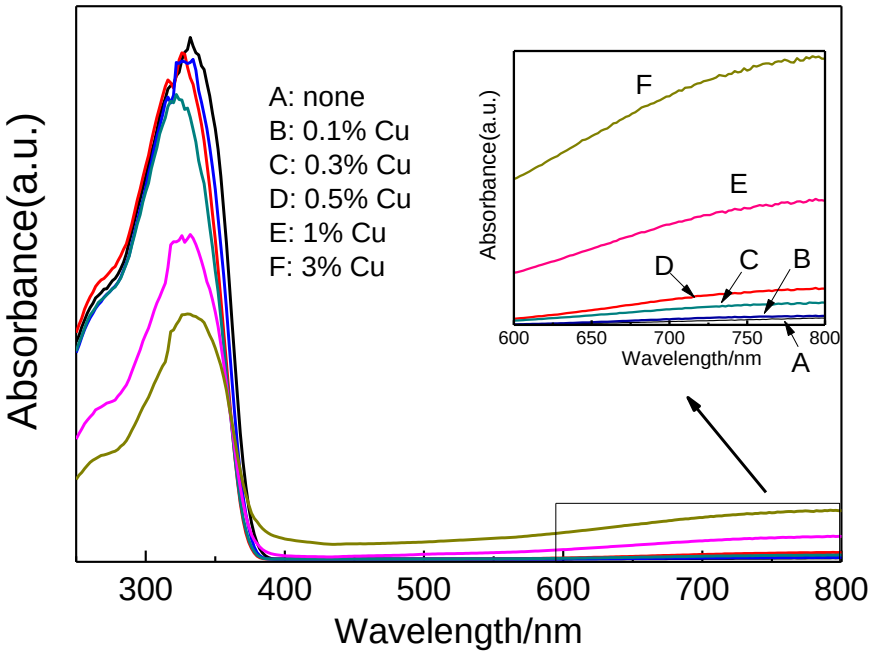

Figure 8

Click here to download Figure: Fig 8.docx

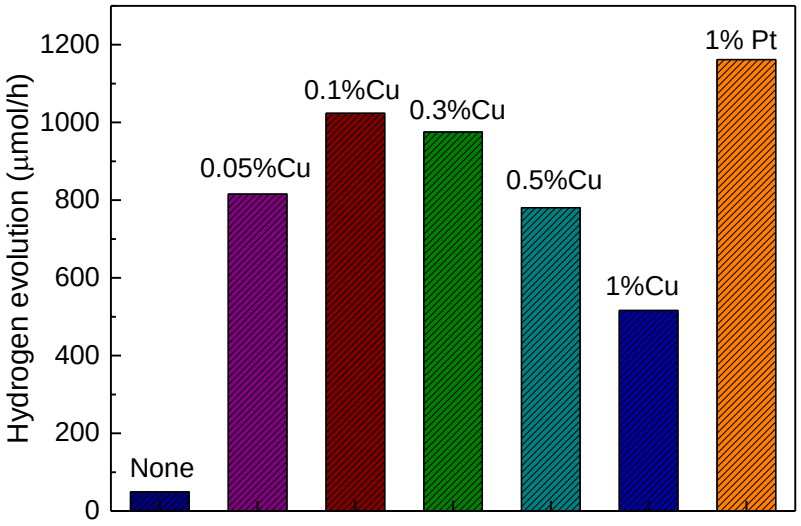

Figure 9

Click here to download Figure: Fig 9.docx

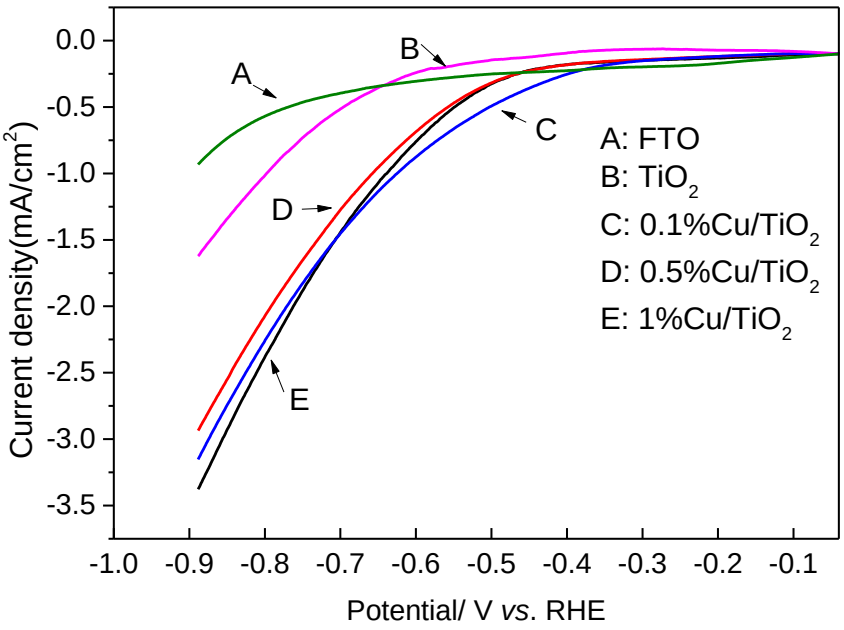

Figure 10

Click here to download Figure: Fig 10.docx